Advances in Bioresearch
Adv. Biores., Vol 17 (2) February 2026: 34-46

Print ISSN 0976-4585; Online ISSN 2277-1573
Journal's URL:http://www.soeagra.com/abr.html
CODEN: ABRDC3
DOI: 10.15515/abr.0976-4585.17.2.3446

Advances in Bioresearch

ORIGINAL ARTICLE

Design, Synthesis, Characterization, Molecular Docking, and ADMET Evaluation of Benzimidazole-Based Derivatives as Potential DNA Gyrase Inhibitors

Smita Kalyanrao Shejul[1]*, Manojkumar Umaji Chopade[2]
[1] Maulana Azad College of Arts, Science and Commerce College, Chhatrapati Sambhajinagar, Maharashtra, India.
[2] Sant Dnyaneshwar Mahavidyalaya College, Soegaon, Maharashtra, India.
***Corresponding author's email:** smitakshejul469@gmail.com

ABSTRACT
The rapid emergence of antimicrobial resistance necessitates the development of new antibacterial agents targeting essential bacterial enzymes. In this study, a series of substituted benzimidazole derivatives (IA–IE) were designed, synthesized, and evaluated as potential Staphylococcus aureus DNA gyrase inhibitors using an integrated experimental and in silico approach. The compounds were synthesized via aldehyde–diamine condensation followed by metal-mediated oxidative cyclization, affording good yields (75–89%), and their structures were confirmed by FTIR, 1H NMR, 13C NMR, and mass spectrometry. Molecular docking studies against DNA gyrase (PDB ID: 7FVS) revealed that the designed derivatives exhibited binding affinities comparable to or better than the native ligand (–6.5 kcal/mol). Among them, compound ID showed the best binding performance with a docking score of –6.9 kcal/mol and the lowest ligand energy (224.37 kcal/mol), forming multiple hydrogen bonds and stabilizing π–π, π–cation, and hydrophobic interactions within the active site. Compounds IB and IC also demonstrated improved docking scores (–6.8 kcal/mol). In silico ADMET analysis indicated that the native ligand displayed poor drug-likeness (QED = 0.095), high polarity (TPSA = 364.15 Å^2), and negligible intestinal absorption. In contrast, the synthesized derivatives showed favorable physicochemical properties (MW 208–316 Da, TPSA 28.68–71.82 Å^2) and improved absorption. Notably, ID exhibited excellent predicted oral absorption (F50% = 0.99) and an acceptable safety profile. Overall, the findings highlight compound ID, followed by IB and IC, as promising lead candidates for further development as DNA gyrase–targeted antibacterial agents.
KEYWORDS: *Benzimidazole derivatives; DNA gyrase inhibition; Molecular docking; ADMET analysis; Antibacterial agents; Staphylococcus aureus.*

Received 24.11.2025 Revised 19.01.2026 Accepted 07.02.2026

How to cite this article:
Smita Kalyanrao S, Manojkumar UC.Design, Synthesis, Characterization, Molecular Docking, and ADMET Evaluation of Benzimidazole-Based Derivatives as Potential DNA Gyrase Inhibitors. Adv. Biores. Vol 17 [2] February 2026. 34-46

INTRODUCTION

The rapid emergence and global spread of antimicrobial resistance (AMR) represent a critical threat to public health, significantly limiting the effectiveness of existing antibiotics and increasing morbidity, mortality, and healthcare costs. Among pathogenic bacteria, *Staphylococcus aureus* remains one of the most challenging organisms due to its ability to acquire resistance against multiple drug classes, including β-lactams, fluoroquinolones, and glycopeptides [1–3]. This alarming scenario underscores the urgent need to identify novel antibacterial agents with new chemical scaffolds and alternative molecular targets capable of overcoming resistance mechanisms. DNA gyrase, a type II topoisomerase unique to bacteria, plays an essential role in DNA replication, transcription, recombination, and chromosome segregation by introducing negative supercoils into DNA. Owing to its absence in higher eukaryotes and its indispensable role in bacterial survival, DNA gyrase has emerged as a highly attractive and validated target for antibacterial drug development [4–6]. Although fluoroquinolones are well-known DNA gyrase inhibitors, their widespread use has led to the rapid development of resistance, primarily through target-site mutations and efflux mechanisms. Consequently, the exploration of non-quinolone scaffolds that can inhibit DNA gyrase through distinct binding interactions has gained considerable research interest.

Benzimidazole and its derivatives constitute an important class of heterocyclic compounds widely recognized for their diverse pharmacological activities, including antibacterial, antifungal, antiviral, anticancer, and anti-inflammatory properties. Structurally, the benzimidazole nucleus resembles purine bases, enabling it to interact effectively with biological macromolecules such as enzymes and nucleic acids [7–9]. This structural versatility, combined with favorable synthetic accessibility and modifiable substitution patterns, makes benzimidazole an attractive scaffold for the design of novel enzyme inhibitors, including those targeting bacterial DNA gyrase [10,11]. Advances in computational chemistry have further accelerated modern drug discovery by enabling the rational design and preclinical evaluation of candidate molecules prior to experimental testing. Molecular docking serves as a powerful tool to predict ligand–protein binding modes, interaction patterns, and relative binding affinities, providing valuable insights into structure–activity relationships. In parallel, in silico ADMET (absorption, distribution, metabolism, excretion, and toxicity) profiling has become an indispensable component of early-stage drug development, allowing the identification of compounds with favorable pharmacokinetic and safety characteristics while reducing late-stage attrition. In this context, the present study focuses on the design, synthesis, characterization, molecular docking, and ADMET evaluation of benzimidazole-based derivatives as potential DNA gyrase inhibitors. A series of structurally diverse benzimidazole analogues were synthesized and thoroughly characterized using spectroscopic techniques to confirm their chemical integrity. Molecular docking studies were employed to explore their binding behavior within the active site of *Staphylococcus aureus* DNA gyrase, while comprehensive ADMET analysis was performed to assess their drug-likeness and pharmacokinetic suitability. This integrated experimental and computational approach aims to identify promising benzimidazole scaffolds that may serve as lead candidates for the development of next-generation antibacterial agents targeting DNA gyrase [12,13].

MATERIAL AND METHODS

All the chemicals used were organic chemical and were purchased from Tokyo Chemical Industry (India) Pvt. Ltd. The Fourier-transform infrared spectroscopy (FTIR) spectrum was performed on Jasco FT/IRb4600 spectrophotometer. Melting points were determined using the Electro-thermal IA 9100 apparatus from Shimadzu. The ^{1}H and ^{13}C NMR spectra were obtained using a Bruker spectrometer in DMSO-d6, CDCl3 Chemical shifts are expressed in δ parts per million relatives to tetramethyl silane (TMS) as the internal standard. All yields refer to the isolated products. The reaction progress was monitored using TLC.

Melting Point Determination

The melting points of the synthesized compounds were determined using an Electrothermal IA 9100 melting point apparatus by the capillary method. Samples were packed into thin-walled capillary tubes and heated gradually until complete melting was observed. The melting points of the synthesized derivatives were found to be in the range of 150–290 °C and are reported without correction. The individual melting point values and percentage yields are summarized in the corresponding table.

Determination of Rf value by Thin layer chromatography (TLC)

Thin layer chromatography was employed to monitor the progress of reactions and to assess the purity of the synthesized derivatives. TLC was performed using silica gel TLC plates-G as the stationary phase. The mobile phase consisted of ethyl acetate and benzene in the ratio of 6:4 (v/v). After development, the chromatographic plates were visualized under ultraviolet (UV) light and in an iodine chamber to detect the separated spots. The Rf values of the synthesized compounds and their corresponding intermediates were calculated using the same solvent system. A clear difference in Rf values between the starting materials and the final products confirmed the successful conversion of reactants into the desired derivatives. The obtained Rf values for derivatives IA–IE are summarized in the corresponding table.

Experimental Procedure for the Synthesis of Benzimidazole Derivatives

O-phenylenediamine (0.01 mol) and the respective substituted benzaldehyde (0.01 mol) was dissolved in 40 mL of ethanol and heated with continuous stirring at 70 °C for 14 to 16 hours. Following the condensation, the mixture was cooled to room temperature, and catalyst $CuCl_2$ (2 g) was added slowly with constant mixing until the reaction medium was just alkaline to litmus, mediating the oxidative cyclization. The crude product was collected by vacuum filtration and washed with ice-cold water. After air-drying for two days, the crude yield was recorded as 50-90%. Purification was performed by recrystallization: the crude product was dissolved in 20 mL of boiling ethanol, and the hot solution was rapidly filtered under vacuum. The filtrate was collected and allowed to cool, precipitating the pure product. The melting point of the purified products was recorded. After determining the melting points, the synthesized products were analyzed by FTIR, NMRs, and Mass for structural confirmation. The detailed reaction scheme used for the synthesis of final derivatives are shown in Figure 1.

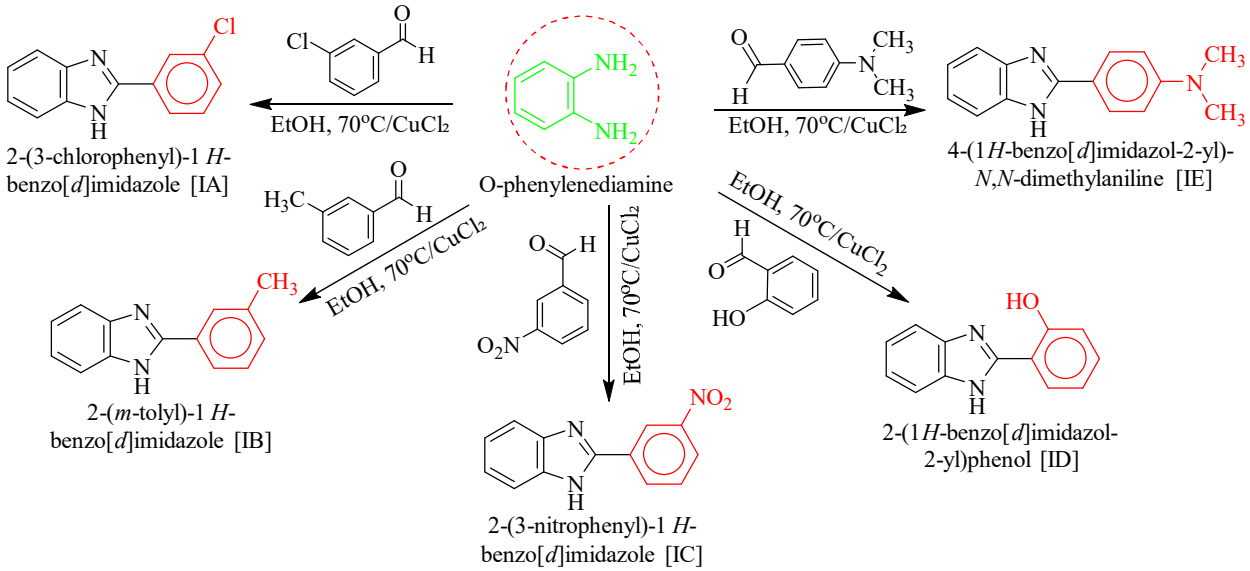

Figure 1: The detailed reaction scheme used for the synthesis of final derivatives

ADMET Analysis

The absorption, distribution, metabolism, excretion, and toxicity (ADMET) profiles of the selected compounds were evaluated using an integrated in silico approach. Initially, the chemical structures of all compounds were drawn and energy-minimized using ChemDraw, and the corresponding SMILES formats were generated for further analysis. Drug-likeness and key pharmacokinetic parameters, including physicochemical properties, oral bioavailability, gastrointestinal absorption, blood–brain barrier permeability, and Lipinski's rule of five compliance, were predicted using the SwissADME web server. SwissADME was also employed to assess solubility, lipophilicity, and bioavailability radar profiles, providing an overall estimation of the compounds' suitability as drug-like candidates. Comprehensive ADMET predictions were further performed using ADMETlab, which was utilized to evaluate absorption parameters (such as human intestinal absorption), distribution characteristics, metabolic behavior (including cytochrome P450 enzyme interactions), excretion properties, and toxicity endpoints (hepatotoxicity, cardiotoxicity, and mutagenicity). The combined use of ChemDraw, SwissADME, and ADMETlab enabled a systematic and reliable assessment of the pharmacokinetic and safety profiles of the selected compounds, supporting their potential for further drug development studies [14–16].

Docking Analysis

Molecular docking studies were performed to investigate the binding interactions between the selected ligands and the target protein (Figure 2). The three-dimensional crystal structure of the target protein was retrieved from the Protein Data Bank (PDB) with the PDB ID 7FVS. The protein structure was prepared using Discovery Studio, where co-crystallized ligands, water molecules, and other heteroatoms were removed, and missing hydrogen atoms were added. Energy minimization was carried out to optimize the protein structure prior to docking. The chemical structures of the selected compounds were drawn using ChemDraw, and the generated structures were converted into appropriate file formats. Ligand preparation, including geometry optimization and energy minimization, was performed before docking. Molecular docking was conducted using PyRx, which employs AutoDock Vina for binding affinity calculations. The active site of the target protein was defined by setting a grid box centered at X = 51.361379, Y = 16.764069, and Z = 25.691207, covering the key residues involved in ligand binding. Docking parameters were kept at default settings to ensure reliable and reproducible results. The docked complexes were analyzed using Discovery Studio to evaluate binding affinities, interaction patterns, hydrogen bonds, hydrophobic interactions, and other non-covalent interactions [17–19]. The docking outcomes provided insights into the binding modes and potential inhibitory mechanisms of the selected compounds against the target protein.

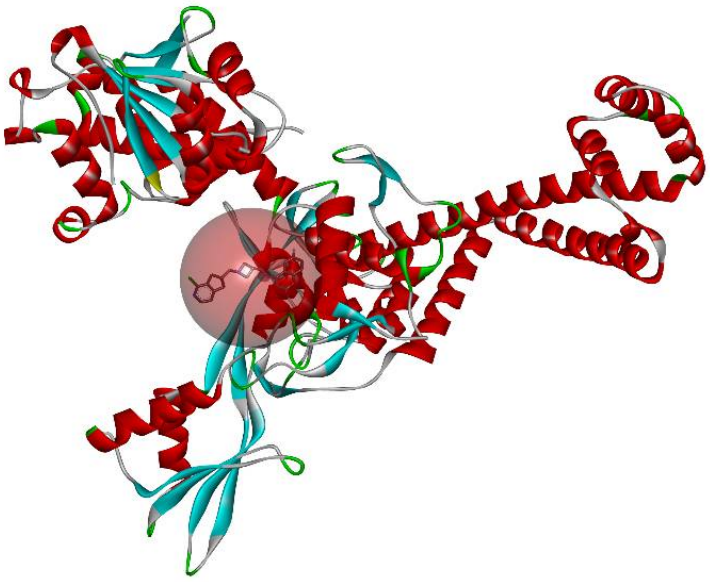

Figure 2: **Active cavity of *Staphylococcus aureus* DNA gyrase with Native ligand in crystal structure with PDB ID of 7FVS**

RESULTS AND DISCUSSION

Chemistry

The present study describes the successful synthesis of a series of benzimidazole derivatives through a classical condensation–oxidative cyclization strategy employing *o*-phenylenediamine and various substituted benzaldehydes. The reaction pathway (Scheme 1) demonstrates the expected formation of benzimidazole scaffolds via initial Schiff base formation followed by intramolecular cyclodehydration and subsequent oxidative aromatization. The use of $CuCl_2$ as the oxidizing catalyst efficiently promoted the transformation under relatively mild conditions (70 °C, ethanol), resulting in good crude yields (50–90%) across all substituent classes.

Analysis of the reaction scheme indicates that electronic effects of substituents played a noticeable role in the progression and cleanliness of the transformations. Electron-withdrawing groups such as 3-chloro and 3-nitro favored smooth Schiff base formation and cyclization, likely due to enhanced electrophilicity of the benzaldehyde carbonyl. These substrates provided benzimidazoles IA and IC in comparatively higher yields with minimal byproduct formation. Conversely, electron-donating groups, such as the m-tolyl substituent, typically stabilize the carbonyl group, slowing imine formation; however, the extended heating period applied in this protocol ensured effective conversion to derivative IB.

The oxidative cyclization step, which converts the diimine intermediate to the fully aromatized benzimidazole nucleus, was consistently efficient under the $CuCl_2$ catalysis conditions. Ethanol served not only as solvent but also as a compatible medium that prevented aldehyde polymerization and supported homogeneous mixing. The gradual addition of catalyst under slightly alkaline conditions helped prevent over-oxidation and minimized tar formation, which is a common challenge in benzimidazole cyclizations.

Purification by hot ethanol recrystallization yielded analytically pure compounds suitable for complete structural characterization. The sharp melting points observed for all derivatives confirmed good purity and supported successful crystallization. Additional spectroscopic analyses (FTIR, NMR, and Mass) confirmed the expected benzimidazole framework, including the characteristic N–H stretching vibration in the FTIR spectra, the disappearance of aldehydic proton signals in NMR, and molecular ion peaks corresponding to the respective substituted benzimidazoles.

Collectively, the synthetic approach demonstrated robustness toward a variety of substituents, and the reaction scheme aligns well with known benzimidazole-forming mechanisms. The successful formation of derivatives IA–ID validates the condensation–cyclization methodology and supports its applicability for generating structurally diverse benzimidazoles for further pharmacological evaluation.

Characterization of synthesized compounds

2-(3-chlorophenyl)-1H-benzo[d]imidazole [IA]

MF: $C_{13}H_9ClN_2$, Rf value: 0.46; m.p.: 290°C; % yield: 85%. FTIR (cm^{-1}): 3054.69 (Ar–C–H stretching), 1671.98 (C=N stretching, heteroaromatic/benzimidazole), 1600.63, 1523.49 (Ar C=C stretching), 1488–1273 (C–N stretching and Ar–C–H bending), 1159–1012 (Ar–C–H in-plane bending), 963.26, 831.69 (Ar–C–H out-of-plane bending), 740.53 (C–Cl stretching), 517.73 (aromatic skeletal vibration). ^{1}H-NMR

(CD_3OD, 600 MHz, δ ppm): 13.18 (1H, s, NH), 8.15–7.52 (Ar–H, m, aromatic protons), ~4.8–4.9 (residual solvent, CD_3OD). ^{13}C-NMR (CD_3OD, 500 MHz, δ ppm): 152.18 (C, C=N/heteroatom-substituted quaternary carbon), 137.31, 133.15, 130.35, 129.68, 127.81, 124.13 (Ar sp^2 carbons); ~49–50 (residual solvent, CD_3OD). MS (m/z): 238.02 gm/mol.

2-(m-tolyl)-1H-benzo[d]imidazole [IB]

MF: $C_{28}H_{28}N_4O$, Rf value: 0.29; m.p.: 280°C; % yield: 75%. FTIR (cm^{-1}): 3338.18 (N–H/O–H stretching, hydrogen-bonded heteroatoms), 2360.44 (atmospheric CO_2), 1737.55 (C=O stretching), 1609.31, 1552.42 (Ar C=C/C=N stretching), 1499.42, 1428.03 (Ar–C–H bending), 1370.18–1272.79 (C–N/C–O stretching), 1163.83, 1108.87, 1063.55 (Ar–C–H in-plane bending), 963.27, 819.59, 741.49 (Ar–C–H out-of-plane bending), 606.50, 543.83 (ring deformation modes). ^{1}H-NMR (CD_3OD, 600 MHz, δ ppm): 13.39 (1H, s, NH), 7.95–7.40 (Ar–H, m, aromatic protons), ~4.8–4.9 (residual solvent, CD_3OD), ~2.39 (trace solvent/impurity). ^{13}C-NMR (CD_3OD, 500 MHz, δ ppm): 151.41, 145.22 (C, deshielded quaternary carbons), 140.00–115.02 (Ar sp^2 carbons), 21.61 (CH_3, aliphatic carbon); ~49–50 (residual solvent, CD_3OD). MS (m/z): 208.02 gm/mol.

2-(3-nitrophenyl)-1H-benzo[d]imidazole [IC]

MF: $C_{26}H_{22}N_6O_5$, Rf value: 0.51; m.p.: 282 °C; % yield: 84%. FTIR (cm^{-1}): 3109.65 (Ar–C–H stretching), 1619.91 (C=C/C=N stretching, conjugated aromatic system), 1517.77 (Ar ring stretching), 1452.28–1434.78 (Ar–C–H bending), 1345.11 (C–N stretching), 1274.72–1136.83 (Ar–C–H in-plane bending), 975.84, 909.27–892.47, 808.98, 761.74, 701.96 (Ar–C–H out-of-plane bending of substituted rings), 557.33 (ring deformation mode). ^{1}H-NMR (DMSO-d_6, 600 MHz, δ ppm): 13.29 (1H, s, NH), 8.42–7.26 (Ar–H, m, aromatic protons), ~3.38 (residual solvent, DMSO-d_6), ~2.51 (residual water in DMSO). ^{13}C-NMR (DMSO-d_6, 500 MHz, δ ppm): 154.22, 149.03, 145.86 (C, deshielded quaternary carbons), 140.00–124.67 (Ar sp^2 carbons), 117.03 (CH, protonated aromatic carbon); ~45–44 (residual solvent, DMSO-d_6). MS (m/z): 232 gm/mol.

2-(1H-benzo[d]imidazol-2-yl)phenol [ID]

MF: $C_{33}H_{30}N_4O_4$, Rf value: 0.41; m.p.: 163°C; % yield: 82%. FTIR (cm^{-1}): 3222.47 (N–H/O–H stretching, hydrogen-bonded heteroatoms), 2360.44 (atmospheric CO_2), 1609.31, 1552.42 (Ar C=C/C=N stretching, conjugated system), 1498.42, 1428.03 (Ar–C–H bending), 1370.18 (C–N stretching), 1272.79–1163.83 (Ar–C–H in-plane bending), 963.27, 818.63, 754.63–723.75 (Ar–C–H out-of-plane bending of substituted rings), 613.25, 543.83 (ring deformation modes). ^{1}H-NMR (DMSO-d_6, 600 MHz, δ ppm): 13.40 (1H, s, NH), 7.90–6.70 (Ar–H, m, aromatic protons), ~2.50 (residual solvent, DMSO-d_6), ~3.30 (trace water in DMSO). ^{13}C-NMR (DMSO-d_6, 500 MHz, δ ppm): 163.70, 160.69 (C, deshielded quaternary aromatic carbons), 147.16–117.09 (Ar sp^2 carbons); ~39–40 (residual solvent, DMSO-d_6). MS (m/z): 213.1 gm/mol.

4-(1H-benzo[d]imidazol-2-yl)-N,N-dimethylaniline [IE]

MF: $C_{30}H_{34}ClCuN_6O$, Rf value: 0.36; m.p.: 285°C; % yield: 89%. FTIR (cm^{-1}): 3221.5 (N–H/O–H stretching, hydrogen-bonded heteroatoms), 2360.44 (atmospheric CO_2), 1607.38 (Ar C=C/C=N stretching, conjugated system), 1498.42, 1437.67 (aromatic ring stretching and Ar–C–H bending), 1361.5 (C–N stretching), 1226.5–1061.62 (Ar–C–H in-plane bending), 944.95, 812.85, 744.39 (Ar–C–H out-of-plane bending of substituted rings), 607.47, 518.75 (ring deformation modes). ^{1}H-NMR (DMSO-d_6, 600 MHz, δ ppm): 13.40 (1H, s, NH), 8.00–6.90 (Ar–H, m, aromatic protons), ~2.50 (residual solvent, DMSO-d_6), ~3.30 (trace water in DMSO). ^{13}C-NMR (DMSO-d_6, 500 MHz, δ ppm): 168.90, 154.30, 152.20 (C, deshielded quaternary aromatic carbons), 134.50–117.40 (Ar sp^2 carbons); ~40.20 (residual solvent, DMSO-d_6). MS (m/z): 237.2 gm/mol.

ADMET Analysis

The native ligand (NL) exhibits an exceptionally high molecular weight (745.09 Da) and TPSA (364.15 Å^2), far exceeding the optimal limits for oral drug candidates (MW < 500 Da; TPSA < 140 Å^2). In addition, NL possesses a very high number of hydrogen bond acceptors (24) and donors (11), along with 13 rotatable bonds, which collectively indicate excessive polarity, poor membrane permeability, and limited oral bioavailability. Its negative logP (–3.25) further confirms its hydrophilic nature, explaining its unfavorable absorption behavior. In contrast, the designed derivatives IA–IE show significantly improved physicochemical profiles. Their molecular weights range from 208.1 to 316.12 Da, TPSA values are reduced to 28.68–71.82 Å^2, and hydrogen bond counts are markedly lower (nHA: 2–5; nHD: 1–2). These values fall well within drug-likeness thresholds. Moreover, the derivatives display optimal lipophilicity with logP values between 3.10 and 4.04, which is favorable for passive diffusion across biological membranes. Among them, ID (MW 316.12 Da, TPSA 65.18 Å^2) and IE (MW 237.13 Da, TPSA 31.92 Å^2) exhibit the best balance between polarity and lipophilicity compared to NL are shown Table 1.

NL shows a very low QED score (0.095), indicating poor overall drug-likeness despite partial compliance with Lipinski and GSK rules. This poor score is consistent with its extreme molecular size and polarity.

Additionally, NL satisfies the chelator and golden triangle rules, but these advantages are outweighed by its unfavorable physicochemical properties. Conversely, derivatives IA–IE demonstrate substantially higher QED values (0.551–0.741), reflecting improved chemical attractiveness as drug candidates. IE shows the highest QED score (0.741), followed by ID (0.691), indicating superior drug-likeness. Although the derivatives violate Lipinski rules due to lipophilicity, they consistently comply with Pfizer rules, suggesting acceptable safety margins during drug development (Table 2). Overall, all designed derivatives exhibit markedly better drug-likeness profiles than NL.

The absorption profile of NL is highly unfavorable, as indicated by poor Caco-2 permeability (–5.84) and MDCK permeability (–5.20), along with extremely low human intestinal absorption (HIA = 0.00015). Fraction absorbed values are almost negligible (F50% = 0.00062), confirming its limited oral bioavailability. In contrast, derivatives IA–IE show improved permeability and absorption. Caco-2 values range from –4.62 to –4.88, and MDCK values from –4.71 to –4.85, indicating enhanced membrane transport compared to NL. Notably, ID exhibits exceptional absorption, with F20%, F30%, and F50% values of 0.964, 0.962, and 0.991, respectively, far exceeding NL. IB, IC, and IE also demonstrate moderate to good absorption (F50% = 0.25–0.55). These results clearly indicate that structural optimization significantly improves intestinal absorption relative to NL are shown as Table 3.

NL shows low plasma protein binding (PPB = 18.98%) and negligible BBB penetration (1.97×10^{-6}), limiting its systemic distribution. Additionally, NL demonstrates minimal interaction with CYP450 enzymes, suggesting poor metabolic engagement. In contrast, IA–IE display very high PPB values (95.99–98.65%), indicating prolonged systemic circulation. BBB penetration is notably higher for IA (0.99) and IB (0.89), whereas ID shows minimal BBB permeation (0.00043), which may be advantageous for non-CNS targets. Metabolism analysis reveals that the derivatives show moderate probabilities of acting as CYP substrates or inhibitors, particularly for CYP3A4 and CYP1A2, but without excessive inhibitory risks (Table 4). Overall, the designed compounds demonstrate more realistic and favorable distribution–metabolism profiles than NL.

NL exhibits low plasma clearance (1.49) and a longer half-life (1.92 h), which may promote drug accumulation and toxicity. Toxicity predictions indicate high risks of drug-induced liver injury (DILI = 0.998), skin sensitization (0.997), respiratory toxicity (0.993), and FDA maximum recommended daily dose (FDAMDD = 0.998), raising serious safety concerns. In comparison, derivatives IA–IE show higher plasma clearance (4.49–8.36) and shorter half-lives (0.56–0.90 h), reducing accumulation risk (Table 5). Importantly, the derivatives display lower hepatotoxicity and acceptable Ames toxicity profiles. ID shows a particularly balanced toxicity profile, with moderate DILI (0.978), low eye corrosion (0.0013), and acceptable acute oral toxicity. These results indicate that the designed derivatives are safer than NL.

Environmental toxicity analysis reveals that NL has very low bioaccumulation potential (BCF = –0.03), but shows comparatively lower LC50 values, indicating higher environmental toxicity. In contrast, derivatives IA–IE exhibit moderate BCF values (1.18–2.22) and higher LC50FM and LC50DM values (4.14–5.50), suggesting reduced environmental risk. Among them, IC and IE demonstrate the most favorable ecological safety profiles are shown Table 6.

Table 1: Physicochemical properties of selected derivatives

Compounds code	MW	Volume	Dense	nHA	nHD	nRot	nRing	TPSA	logS	logP
NL	745.09	596.4276	1.249255	24	11	13	5	364.15	-1.7211	-3.2486
IA	228.05	226.4843	1.006913	2	1	1	3	28.68	-5.01648	4.0425
IB	208.1	228.5692	0.910446	2	1	1	3	28.68	-4.26878	3.518617
IC	239.07	237.214	1.007824	5	1	2	3	71.82	-4.58583	3.103793
ID	316.12	339.3797	0.931464	4	2	4	3	65.18	-4.27332	3.965413
IE	237.13	256.8619	0.923181	3	1	2	3	31.92	-3.71477	3.223184

Table 2: Drug-likeness properties of designed derivatives

Compounds code	QED	NP Score	Lipinski rule	Pfizer Rule	GSK Rule	Golden Triangle	Chelator Rule
NL	0.095	0.984	1	0	1	1	1
IA	0.673	-1.365	0	1	1	0	0
IB	0.651	-1.19	0	1	0	0	0
IC	0.551	-1.475	0	1	0	0	0
ID	0.691	-0.356	0	1	0	0	0
IE	0.741	-1.31	0	1	0	0	0

Table 3: Absorption parameter of selected compounds

Compounds code	Caco-2 Permeability	MDCK Permeability	Pgp-inhibitor	Pgp-substrate	HIA	F20%	F30%	F50%
NL	-5.835687411	-5.199739162	3.58E-05	1.34E-10	0.000149846	0	0.006481707	0.000624597
IA	-4.62424	-5.00003	0.781672	0.017688	0.000325	0.008385	0.013894	0.159853
IB	-4.85429	-4.84719	0.89081	0.065028	0.000859	0.078066	0.056037	0.277729
IC	-4.87606	-4.71583	0.379988	0.015229	0.001436	0.039023	0.070424	0.251277
ID	-4.81127	-4.77556	0.046596	3.01E-06	0.007919	0.963985	0.961771	0.990698
IE	-4.71955	-4.85466	0.893505	0.228503	0.006425	0.111062	0.14016	0.553301

Table 4: Distribution and metabolism parameter of selected molecules

Compounds code	Distribution				Metabolism									
					CYP1A2		CYP2C19		CYP2C9		CYP2D6		CYP3A4	
	PPB%	VD	BBB	Fu	Inhibitor	Substrate	Inhibitor	Substrate	Inhibitor	Substrate	Inhibitor	Substrate	Inhibitor	Substrate
NL	18.98093925	-0.705009489	1.97E-06	62.52330308	5.44E-15	8.62E-23	7.23E-17	1.83E-19	7.04E-06	0.001350455	7.79E-06	1.21E-12	1.41E-11	2.98E-13
IA	98.65159	-0.04663	0.991708	0.739137	0.99965	0.971004	0.936534	0.519686	0.89209	0.006348	0.056281	0.004533	0.024214	0.620422
IB	98.36924	-0.05562	0.885482	1.022724	0.714097	0.994045	0.39169	0.10191	0.90592	0.001143	0.000134	0.000866	0.029978	0.343515
IC	95.98991	-0.03431	0.197058	4.168591	0.494947	0.999973	0.828891	0.020224	0.024349	0.000136	0.000588	0.001414	0.638331	0.002013
ID	97.8375	-0.29556	0.00043	1.943963	0.997717	0.036612	0.486649	4.66E-05	0.7656	0.01049	0.027639	0.002366	0.000964	0.003482
IE	98.20511	0.187867	0.165491	1.500697	0.912728	0.99853	0.9577	0.008501	0.222315	2.20E-05	0.015061	0.000301	0.05703	0.001696

Table 5: Excretion and Toxicity parameters of selected compounds

Compounds code	Excretion		Toxicity									
	CL-plasma	T1/2	H-HT	DILI	Ames Toxicity	Rat Oral Acute Toxicity	FDAMDD	Skin Sensitization	Carcinogenicity	Eye Corrosion	Eye Irritation	Respiratory Toxicity
NL	1.488110107	1.917223383	0.047131952	0.998237133	0.026296746	0.018619854	0.99803561	0.996928036	0.768207371	3.05E-07	0.212988392	0.993361592
IA	5.100458	0.752386	0.635895	0.839829	0.643407	0.526925	0.615347	0.764223	0.645845	0.024733	0.973732	0.847485
IB	6.207348	0.85431	0.648779	0.688257	0.766531	0.444445	0.592788	0.745693	0.703941	0.055568	0.99104	0.886459
IC	4.490841	0.89923	0.745637	0.989027	0.965264	0.639965	0.670147	0.946968	0.797604	0.030592	0.995389	0.960499
ID	8.364774	0.73914	0.915577	0.977971	0.875083	0.128078	0.546469	0.963105	0.918581	0.001303	0.989056	0.671887
IE	7.024158	0.557664	0.637124	0.786437	0.869797	0.613335	0.448325	0.547432	0.915831	0.035012	0.996479	0.987709

Table 6: Environmental toxicity profile of designed molecules

Compounds code	BCF	IGC50	LC50FM	LC50DM
NL	-0.031202046	2.370147484	3.532263287	3.803765975
IA	2.216867	4.226314	5.065791	5.409663
IB	1.582278	4.024913	4.577589	4.592979
IC	1.182264	4.099933	4.568959	4.785158
ID	1.208526	4.440156	5.231111	5.502554
IE	1.227241	3.736121	4.144593	4.560272

Table 7: ADMET radar of most potent compounds and Native ligand

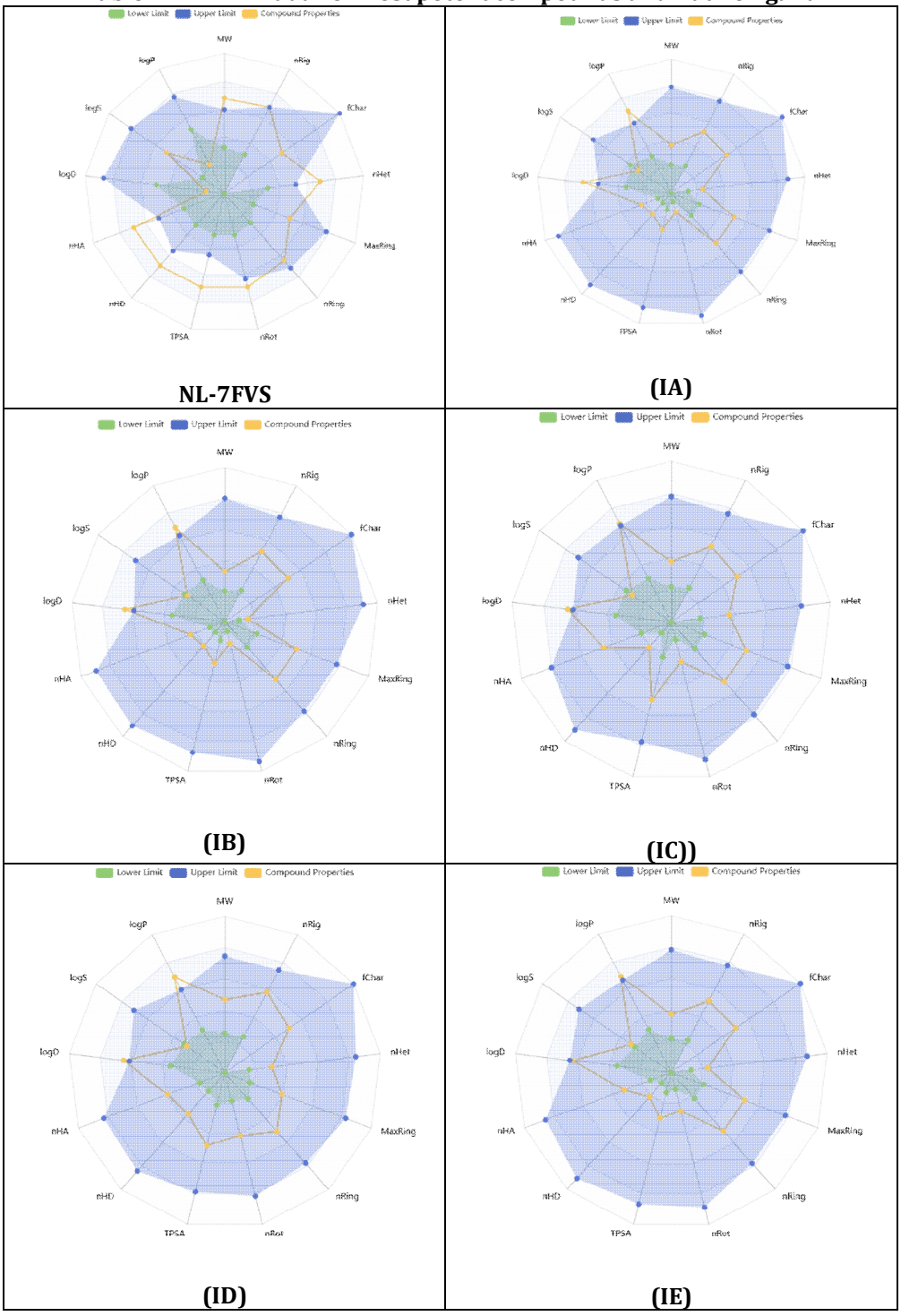

NL-7FVS **(IA)**

(IB) **(IC))**

(ID) **(IE)**

Molecular Docking Analysis

Molecular docking analysis was performed to elucidate the binding behavior and interaction profiles of the selected compounds within the active site of *Staphylococcus aureus* DNA gyrase (PDB ID: 7FVS). The docking scores and interaction patterns indicate notable differences in binding affinity and stabilization mechanisms among the native ligand and the designed compounds (Table 8). The native ligand (NL) exhibited a docking score of −6.5 kcal/mol with a high ligand energy of 2253.24 kcal/mol, reflecting moderate binding affinity. (Table 7) NL formed an extensive network of conventional hydrogen bonds with key active-site residues, including GLU1088, ASP1116, SER1085, ARG1092, GLN1267, and ASN1269, highlighting the importance of polar interactions in anchoring the ligand. Additional carbon hydrogen bonds with SER1085 and GLY1115, along with hydrophobic alkyl interactions involving ARG1033 and ALA1034, further contributed to the stabilization of the ligand within the gyrase binding pocket. Compound IA showed a slightly improved docking score (−6.6 kcal/mol) and a substantially lower ligand energy (334.36 kcal/mol) compared to NL, indicating a more energetically favorable complex. Its binding was predominantly driven by hydrophobic interactions, including π−sigma and alkyl contacts with VAL1091 and ALA1118, as well as π−alkyl interactions with ARG1092, suggesting effective accommodation within the hydrophobic region of the active site. Similarly, IB demonstrated enhanced binding affinity with a docking score of −6.8 kcal/mol. The interaction profile of IB was characterized by consistent π−sigma, alkyl, and π−alkyl interactions with VAL1091, ALA1118, and ARG1092, indicating improved hydrophobic complementarity and tighter binding compared to IA and the native ligand. Compound IC also achieved a docking score of −6.8 kcal/mol, with its binding largely stabilized through π−alkyl interactions with ARG1092, supported by hydrophobic contacts with VAL1091 and ALA1118. The absence of hydrogen bonding suggests that IC relies primarily on hydrophobic forces to maintain binding stability within the gyrase active site. Notably, ID emerged as the most promising candidate, exhibiting the highest docking score of −6.9 kcal/mol and the lowest ligand energy (224.37 kcal/mol) among all tested compounds. ID formed multiple conventional hydrogen bonds with SER1085, indicating strong and specific polar interactions. In addition, electrostatic π−cation interactions with HIS1081, along with π−π stacked and T-shaped interactions involving HIS1081 and HIS1079, and π−alkyl interactions with ARG1033, VAL1045, and ALA1089, collectively enhanced the stability and binding strength of the complex. Compound IE displayed a docking score of −6.6 kcal/mol, comparable to IA and NL. Its interaction pattern included carbon hydrogen bonding and π−anion electrostatic interactions with GLU1088, as well as π−alkyl hydrophobic interactions with ARG1092 and VAL1091, indicating a balanced contribution of polar and hydrophobic forces to binding. Overall, the docking results demonstrate that the designed compounds, particularly ID, followed by IB and IC, exhibit equal or superior binding affinity compared to the native ligand toward *Staphylococcus aureus* DNA gyrase. The improved interaction profiles, involving a synergistic combination of hydrogen bonding, electrostatic, and hydrophobic interactions, suggest that these compounds—especially ID—may serve as promising lead candidates for the development of novel DNA gyrase inhibitors. The 2D and 3D binding interaction poses of the most potent Compounds with *Staphylococcus aureus* DNA gyrase are shown in Table 9.

Table 8: Binding interactions of selected compounds with *Staphylococcus aureus* DNA gyrase

Amino Acid	Bond Length	Bond Type	Bond Category	Ligand Energy (Kcal/mol)	Docking Score (Kcal/mol)
NL					
GLU1088	2.96382	Hydrogen Bond	Conventional Hydrogen Bond	2253.24	-6.5
ASP1116	2.48484				
SER1085	2.03241				
ARG1092	1.90792				
GLN1267	2.26115				
GLN1267	2.27452				
GLN1267	2.82554				
ASN1269	2.36696				
ASN1269	2.27006				
SER1085	3.69737		Carbon Hydrogen Bond		
GLY1115	3.7065				
GLY1115:	3.49766				
GLY1115	3.33258				
ARG1033	5.36628	Hydrophobic	Alkyl		

ALA1034	5.458				
IA					
VAL1091	3.9124	Hydrophobic	Pi-Sigma	334.36	-6.6
VAL1091	4.0238		Alkyl		
ALA1118	3.7317				
ARG1092	5.04857		Pi-Alkyl		
ARG1092	5.29178				
ALA1118	5.27998				
IB					
VAL1091	3.95251	Hydrophobic	Pi-Sigma	335.14	-6.8
VAL1091	4.02677		Alkyl		
ALA1118	3.78871				
ARG1092	5.09935		Pi-Alkyl		
ARG1092	5.33002				
ALA1118	5.29376				
IC					
ARG1092	4.95576	Hydrophobic	Pi-Alkyl	347.87	-6.8
VAL1091	4.68638				
ARG1092	5.34887				
ALA1118	5.33834				
ID					
SER1085	2.44268	Hydrogen Bond	Conventional Hydrogen Bond	224.37	-6.9
SER1085	2.46488				
SER1085	2.00113				
HIS1081	4.64438	Electrostatic	Pi-Cation		
HIS1081	5.73629	Hydrophobic	Pi-Pi Stacked		
HIS1079	4.55447		Pi-Pi T-shaped		
ARG1033	3.88276		Pi-Alkyl		
VAL1045	4.70168				
ALA1089	5.05966				
IE					
GLU1088	3.59013	Hydrogen Bond	Carbon Hydrogen Bond	354.42	-6.6
GLU1088	4.80469	Electrostatic	Pi-Anion		
ARG1092	5.10198	Hydrophobic	Pi-Alkyl		
VAL1091	4.94873				

Table 9: The 2D and 3D binding interaction poses of the most potent Compounds with *Staphylococcus aureus* DNA gyrase

3D Binding Interaction	2D Binding Interaction
NL -7FVS	
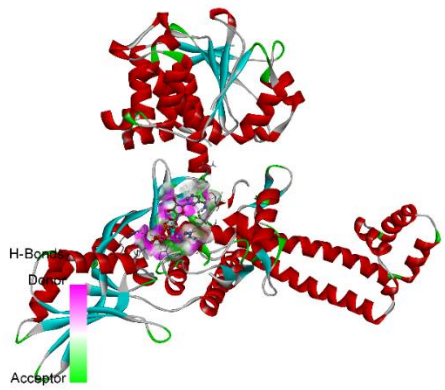	Not Generated by the software
(IA)	

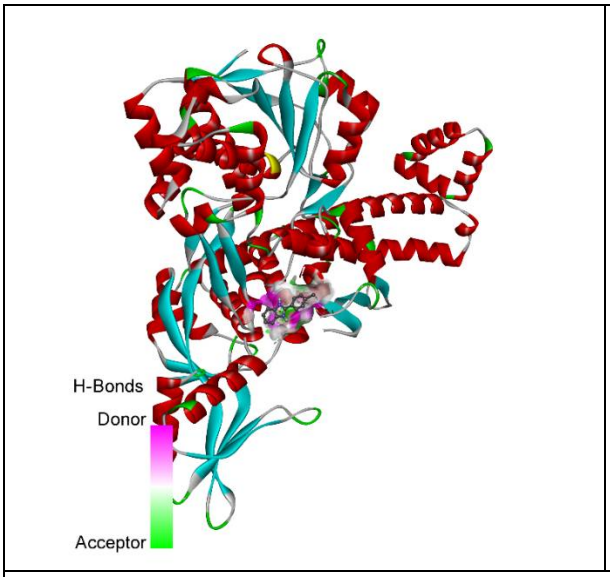
H-Bonds
Donor
Acceptor

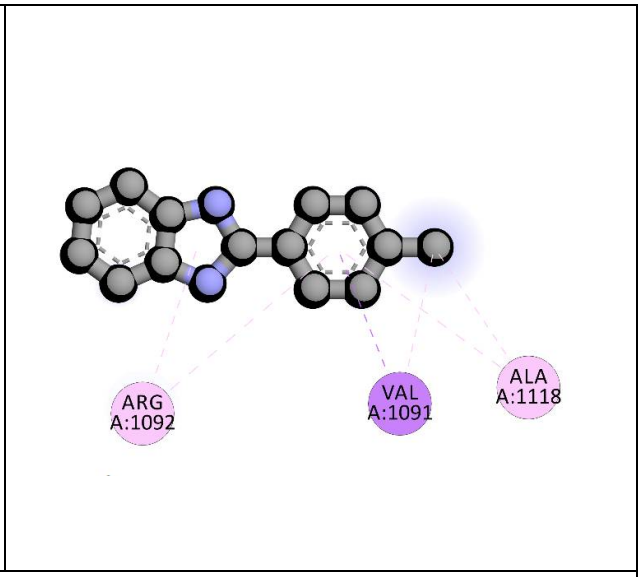
ARG
A:1092
VAL
A:1091
ALA
A:1118

(IB)

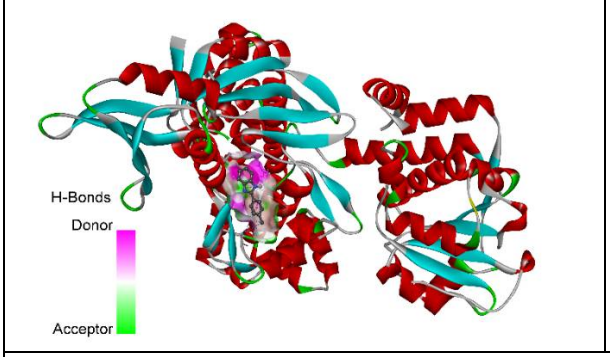
H-Bonds
Donor
Acceptor

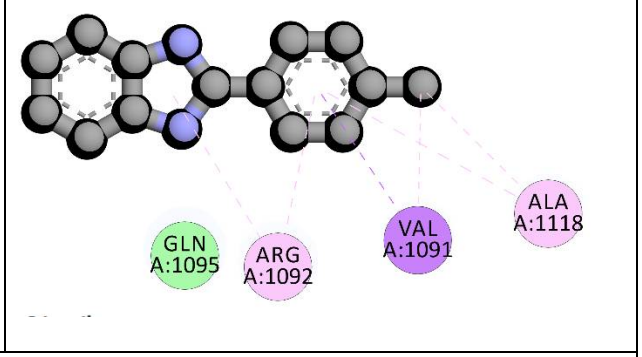
GLN
A:1095
ARG
A:1092
VAL
A:1091
ALA
A:1118

(IC)

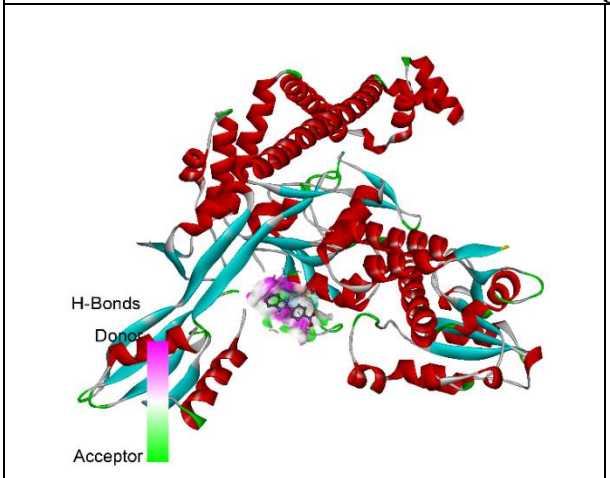
H-Bonds
Donor
Acceptor

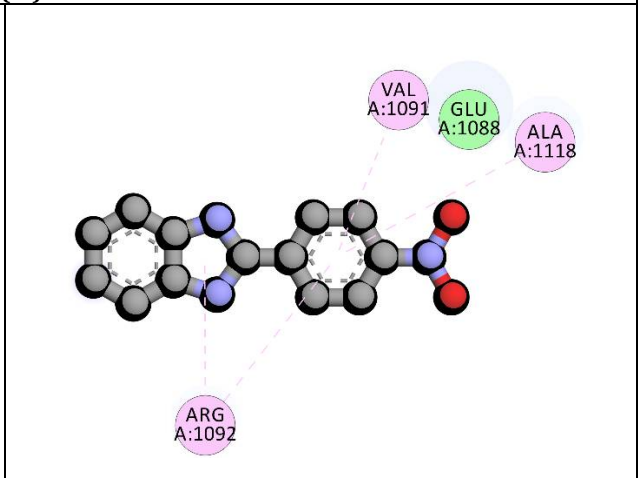
VAL
A:1091
GLU
A:1088
ALA
A:1118
ARG
A:1092

(ID)

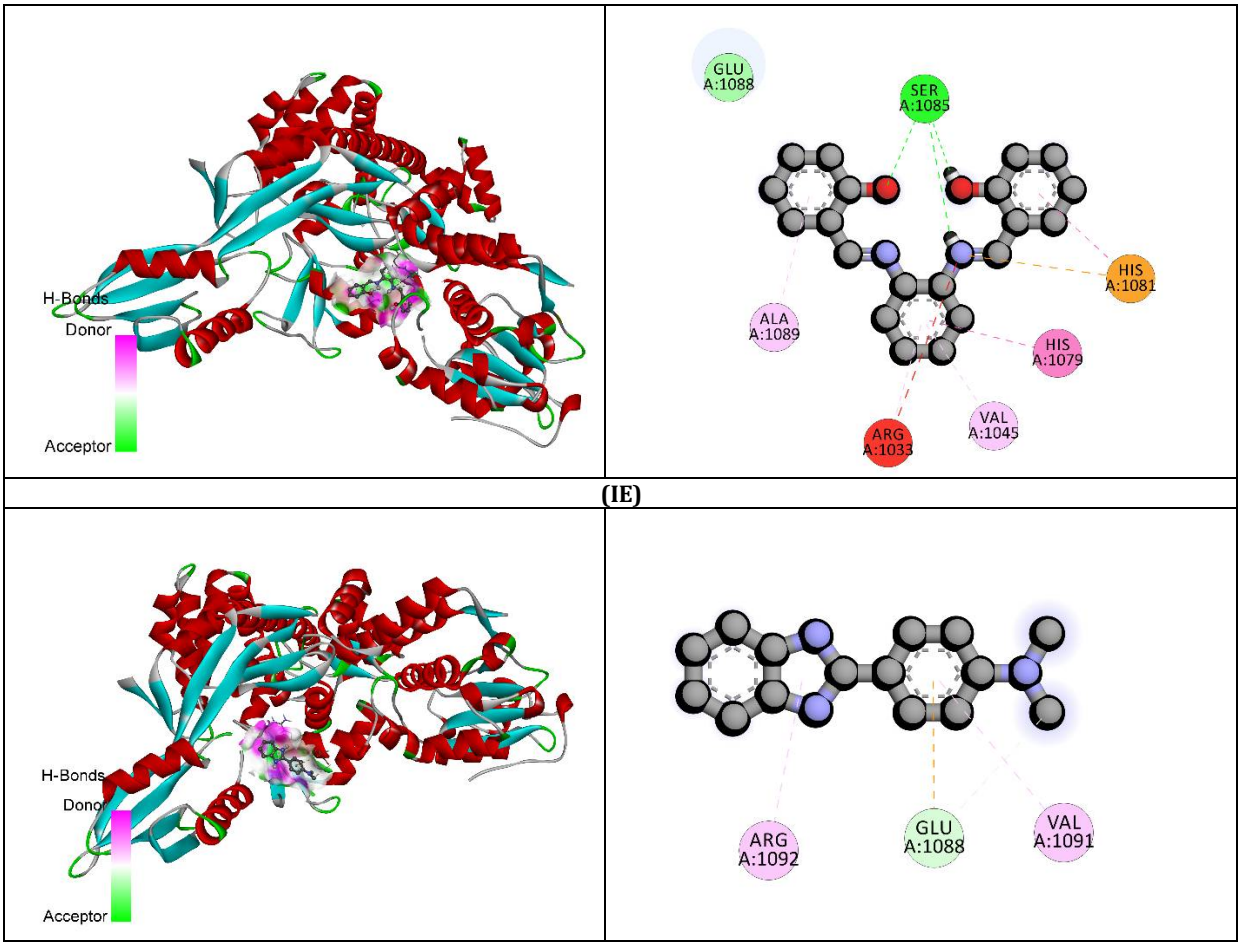

(IE)

CONCLUSION

In the present study, a series of benzimidazole-based derivatives (IA–IE) were successfully designed, synthesized, and comprehensively evaluated as potential inhibitors of *Staphylococcus aureus* DNA gyrase through an integrated experimental and in silico approach. The synthetic strategy employing aldehyde–diamine condensation followed by metal-mediated oxidative cyclization afforded the target compounds in good to excellent yields, and their structures were unequivocally confirmed by FTIR, 1H NMR, 13C NMR, and mass spectrometric analyses. Molecular docking studies against DNA gyrase (PDB ID: 7FVS) demonstrated that the designed compounds exhibit comparable or improved binding affinities relative to the native ligand. Among them, compound ID emerged as the most promising candidate, displaying the highest docking score (–6.9 kcal/mol), the lowest ligand energy, and a rich interaction profile involving hydrogen bonding, π–π stacking, π–cation, and hydrophobic interactions within the active site. Furthermore, ADMET evaluation revealed that the native ligand suffers from poor drug-likeness, unfavorable absorption, and high toxicity risks, whereas the designed derivatives show significantly improved physicochemical properties, enhanced intestinal absorption, acceptable metabolic behavior, and safer toxicity profiles. Notably, compounds ID and IE demonstrated an optimal balance between permeability, safety, and pharmacokinetic feasibility, while also exhibiting reduced environmental toxicity. Overall, the combined results highlight ID, followed by IB and IC, as promising lead molecules for further optimization and experimental validation as novel DNA gyrase inhibitors, supporting their potential development as antibacterial agents.

ACKNOWLEDGMENTS

G.N.W. is gratefully thankful to the Chhatrapati Shahu Maharaj Research, Training and Human Development Institute (SARTHI), Pune for CSMNRF-July-2022, Junior Research Fellowship.

REFERENCES

1. Massé J, Vanier G, Fairbrother JM, de Lagarde M, Arsenault J, Francoz D, et al. (2023).Description of Antimicrobial-Resistant Escherichia coli and Their Dissemination Mechanisms on Dairy Farms. Vet Sci.;10(4).

2. Laffont-Lozes P, Larcher R, Salipante F, Leguelinel-Blache G, Dunyach-Remy C, Lavigne JP, et al. (2023). Usefulness of dynamic regression time series models for studying the relationship between antimicrobial consumption and bacterial antimicrobial resistance in hospitals: a systematic review. Vol. 12, Antimicrobial Resistance and Infection Control.
3. Young CCW, Karmacharya D, Bista M, Sharma AN, Goldstein T, Mazet JAK, et al. (2022). Antibiotic resistance genes of public health importance in livestock and humans in an informal urban community in Nepal. Sci Rep.12(1).
4. Papillon J, Ménétret JF, Batisse C, Hélye R, Schultz P, Potier N, et al. (2013). Structural insight into negative DNA supercoiling by DNA gyrase, a bacterial type 2A DNA topoisomerase. Nucleic Acids Res.41(16):7815–27.
5. Higgins NP. (2016). Species-specific supercoil dynamics of the bacterial nucleoid. Biophys Rev.;8. 20;8(Suppl 1):113–121. doi: 10.1007/s12551-016-0207-9
6. Zechiedrich EL, Khodursky AB, Cozzarelli NR. (1997). Topoisomerase IV, not gyrase, decatenates products of site-specific recombination in Escherichia coli. Genes Dev. 11(19):2580–92.
7. Ulanowska M, Olas B.(2021). Biological properties and prospects for the application of eugenol—a review. Vol. 22, International Journal of Molecular Sciences.
8. Shuai H, Myronovskyi M, Nadmid S, Luzhetskyy A. (2020). dentification of a biosynthetic gene cluster responsible for the production of a new pyrrolopyrimidine natural product—huimycin. Biomolecules.10(7):1–10.
9. Ben Miri Y.(2025). Essential Oils: Chemical Composition and Diverse Biological Activities : A Comprehensive Review. Vol. 20, Natural Product Communications.
10. Singla P, Luxami V, Paul K. (2014). Benzimidazole-biologically attractive scaffold for protein kinase inhibitors. Vol. 4, RSC Advances. p. 12422–40.
11. Singh K, Bhushan B, Varma AK, Shekhar R, Sharma RK, Ghosh NS, et al.(2024). A Comprehensive Review of the Benzimidazole Scaffold as a Potential Nucleus for Anti-Ulcer Activity. Vol. 21, Letters in Organic Chemistry. p. 493–504.
12. Herqash RN, Alanzi AR, Ahamad SR, Rehman MT, Alharbi MS, Alsufyani SA, et al.(2024). Exploring the phytochemical profile and antioxidant evaluation: Molecular docking and ADMET analysis of main compounds from three Solanum species in Saudi Arabia. Open Chem.22(1).
13. Abu-Hashem AA, Amri N, El-Sayed AF. (2025). Design, evaluation, cytotoxic activity, molecular docking, ADMET analysis, and dynamic simulations and the preparation of new isoxazoles, thiazoles, 1,3-thiazines, and thiazolopyrimidines derived from quinoline-pyridopyrimidines. Pharm Biol.63(1):607–44.
14. Gandla K, Islam F, Zehravi M, Karunakaran A, Sharma I, Haque MA, et al. (2023). Natural polymers as potential P-glycoprotein inhibitors: Pre-ADMET profile and computational analysis as a proof of concept to fight multidrug resistance in cancer. Heliyon.9(9). 90
15. Shaheen A, Fida H, Akhmedov S, Rasulbek E, Ataullaev Z. (2025). In Silico Study of Alkaloids as Potential Cyclin-Dependent Kinase (CDK) Inhibitors. J Pharm Sci Comput Chem [Internet].1(4):324–35. Available from: https://jpscc.samipubco.com/article_235766_f9de3c3b67552b56d5e748fb40a24329.pdf
16. Joshi M, Pathan I, Sahu A, Raza A, Sahu Y, Khatoon N. (2025). Computational Chemistry in Structure-Based Drug Design: Tools, Trends, and Transformations. J Pharm Sci Comput Chem.1(3):246–66.
17. Khan SL, Siddiqui FA, Jain SP, Sonwane GM. Discovery of Potential Inhibitors of SARS-CoV-2 (COVID-19) Main Protease (Mpro) from Nigella Sativa (Black Seed) by Molecular Docking Study. Coronaviruses. 2021;2(3):384–402.
18. Chaudhari RN, L.Khan S, Chaudhary RS, Jain SP, Sidduqui FA.(2020). B-Sitosterol: Isolation From *Muntingia Calabura* Linn Bark Extract, Structural Elucidation And Molecular Docking Studies As Potential Inhibitor of Sars-CoV-2 Mpro (COVID-19). Asian J Pharm Clin Res.204–9.
19. Khan A, Unnisa A, Sohel M, Date M, Panpaliya N, Saboo SG, et al. (2021). Investigation of phytoconstituents of Enicostemma littorale as potential glucokinase activators through molecular docking for the treatment of type 2 diabetes mellitus. Silico Pharmacol. Dec10(1):1. 178-189